Theory and simulation of the dynamics, deformation, and breakup of a chain of superparamagnetic beads under a rotating magnetic field

A. Vázquez-Quesada, T. Franke, and M. Ellero

Citation: Physics of Fluids **29**, 032006 (2017); doi: 10.1063/1.4978630
View online: http://dx.doi.org/10.1063/1.4978630
View Table of Contents: http://aip.scitation.org/toc/phf/29/3
Published by the American Institute of Physics

Theory and simulation of the dynamics, deformation, and breakup of a chain of superparamagnetic beads under a rotating magnetic field

A. Vázquez-Quesada,[1] T. Franke,[2] and M. Ellero,[1,a)]
[1]*Zienkiewicz Centre for Computational Engineering (ZCCE), Swansea University, Bay Campus, Swansea SA1 8EN, United Kingdom*
[2]*Division of Biomedical Engineering, School of Engineering, University of Glasgow, Oakfield Avenue, Glasgow G12 8LT, United Kingdom*

(Received 11 October 2016; accepted 2 March 2017; published online 24 March 2017)

In this work, an analytical model for the behavior of superparamagnetic chains under the effect of a rotating magnetic field is presented. It is postulated that the relevant mechanisms for describing the shape and breakup of the chains into smaller fragments are the induced dipole-dipole magnetic force on the external beads, their translational and rotational drag forces, and the tangential lubrication between particles. Under this assumption, the characteristic S-shape of the chain can be qualitatively understood. Furthermore, based on a straight chain approximation, a novel analytical expression for the critical frequency for the chain breakup is obtained. In order to validate the model, the analytical expressions are compared with full three-dimensional smoothed particle hydrodynamics simulations of magnetic beads showing excellent agreement. Comparison with previous theoretical results and experimental data is also reported. *Published by AIP Publishing.* [http://dx.doi.org/10.1063/1.4978630]

I. INTRODUCTION

Superparamagnetic microbeads have been proven to enable manipulation in microfluidic systems and lab on a chip applications by enhancing a number of operations including mixing, separation, and labelling. In a constant external magnetic field $\boldsymbol{B}$, it is well known that they align forming long chains. Such a kind of aggregation is limited when the magnetic field is rotating: there is a competition between magnetic and viscous forces, which determines the dynamics of the system.

Experimentally, these kinds of systems have been typically studied through optical methods such as video microscopy[1–6] or light scattering.[7–10] Experiments show that for very low frequencies, the aggregation process increases.[3,5] At higher frequencies, the size of the chains diminishes until some critical frequency f_0 is reached. Above f_0 a different regime is observed because the aggregation process is prevented due to the fast rotation of the field.[3–5,9,10] From individual observations, the chains under a rotating magnetic field show a typical S-shape and, if the frequency is high enough, they will eventually break up into smaller fragments in order to reduce their viscous drag.[11] The critical frequency which determines the rupture of the chain depends on the frequency of rotation, viscosity, and magnetization.[12–16]

There have also been several theoretical approaches to study the dynamics of these systems. Melle *et al.*[9] model the chain as a cylinder in order to calculate the phase lag. In another work, Melle and Martin[12] studied the behavior of the chain through the Mason number Mn in order to predict its stability and developed an iterative method in order to predict the S-shape. Cēbers and Javaitis[13] developed a mathematical analysis of the rotation of an inextensible flexible magnetic rod under the effect of a rotating field. Such a model captures short and long range magnetic interactions and allows to find a similar scaling on the Mason number of the number of beads, $N \sim 1/\sqrt{\mathrm{Mn}}$, in agreement with other studies.[12] Petousis *et al.*[14] presented a simplified model of linear chain where it is assumed that the relevant part of the magnetic torque is applied by the external particles of the chain, neglecting the contribution torque of the internal ones. In order to test the model, the authors developed a numerical method to simulate chains represented by a pin-jointed mechanism. Rupture of the chain is explained in terms of the tension of the bar, i.e., when it overcomes the attracting force between the beads. Another model to calculate the critical breakup frequency of the chains has been developed by Franke *et al.*[15] In that model, the critical condition for instability requires that the tangential drag force (responsible for disaggregation) is balanced by the attractive dipole-dipole force acting between the beads. When the drag force on extreme beads is close to the magnetic attraction, the chain will deform first, adopting an S-shape, and it will eventually break when the magnetic attraction force is overcome by the viscous force. It must be remarked, however, that in this model, forces with different orientations are compared which is strictly only valid for strongly deformed S-shaped chains so that magnetic and drag forces are antiparallel. Yet, in this model the S-shape chain deformation has not been taken into account and a simple extension can not explain the experimental and numerical evidences that show

a)Author to whom correspondence should be addressed. Electronic mail: M.Ellero@swansea.ac.uk

the chain bends towards the direction of rotation.[12,14,16] In the numerical model presented by Gao *et al.*,[16] the authors consider the hydrodynamic interactions (HIs) by using Rotne-Prage-Yamakawa and Öttinger tensors. It is important to point out that in none of these models lubrication forces between the beads of the chain are considered. However, it is well-known that for very close beads, lubrication forces are much stronger than the far-field hydrodynamic interactions[17] and therefore it is crucial to take them into account for a quantitative description of the problem.

In this work, a new lubrication-based model of linear magnetic chain is presented, which is able to predict the critical frequency of instability and its general rotating dynamics. The incorporation of lubrication effects allows us to understand qualitatively the morphology of the chain and to predict its breakup quantitatively.

In Sec. II the mathematical details of the model are presented. First, S-shape and breakup are explained (Sec. II A). Later, in Sec. II B, the critical frequency for the rupture of the chain is calculated considering translational and rotational friction as well as lubrication forces between particles. In Sec. III the Smoothed Particle Hydrodynamics (SPH) method is used to test the results of the analytical model. Finally, in Secs. IV and V, the new model is compared with the numerical results as well as with existing models and experimental results from the literature.

II. MATHEMATICAL MODEL OF CHAIN DYNAMICS UNDER A ROTATING MAGNETIC FIELD

A spatially homogeneous rotating magnetic field of the form $\boldsymbol{B} = B_0(\cos(\omega t), 0, \sin(\omega t))$ is considered explicitly and its effect on the chain's dynamics is explored. It is assumed that rotation takes place on a plane (x, z) with angular frequency ω and that the most relevant forces involved in the rotation, shape, and breakup of the chain are the magnetic torque of the two external particles and the drag force. The effect of the tangential lubrication force between the beads, which becomes particularly relevant for short chains, is also considered. A detailed analysis of the dynamics of the chain and the calculation of the critical frequency of the chain are performed in Sections II A and II B. Theoretical results will be validated by the direct numerical simulation in Section IV.

A. Chain deformation: S-shape and breakup

In this section, the model is presented and is shown that it is able to predict quantitatively the typical S-shape chain deformation and its breakup.

It is considered that the most relevant interactions in the chain are due to magnetic and friction torques (Fig. 1). When the solid beads are superparamagnetic, the presence of an external magnetic field **B** will induce a magnetic dipole moment. It is also considered that the alignment of the magnetic moment $\boldsymbol{m}_\alpha$ of a given solid bead α with the external magnetic field is fast enough, so it can be taken as instantaneous, in such a way that

$$\boldsymbol{m}_\alpha = \frac{V_c \chi}{\mu_0} \boldsymbol{B}_\alpha, \tag{1}$$

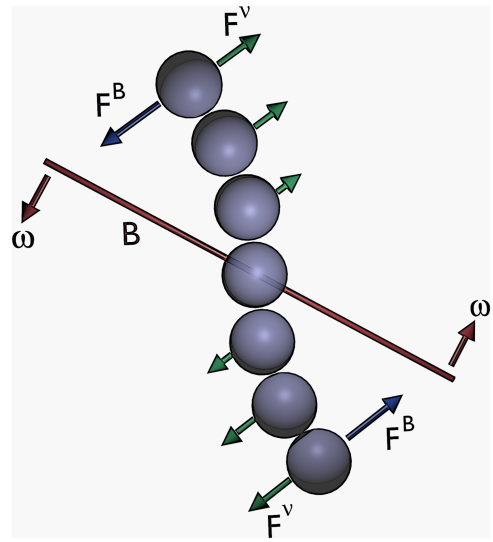

FIG. 1. Scheme of the interactions on the rotating chain. The magnetic field B (red) is rotating with a frequency ω. The interaction driving the alignment of the chain with the magnetic field is the perpendicular component of the magnetic force on the external beads (blue). The viscous force due to the presence of the solvent medium (green) is opposing to the alignment of the chain. The drag torque coming from the rotation of the spheres around their own axis has not been represented.

where $V_c = 4\pi a^3 f/3$ is the volume of a paramagnetic bead of radius a, with f being the fraction of the bead's volume that is paramagnetic and $\boldsymbol{B}_\alpha$ the magnetic field estimated at the bead's position $\boldsymbol{R}_\alpha$. χ is the magnetic susceptibility difference between the bead and the suspending fluid, whereas μ_0 is the vacuum magnetic permittivity. The approximation (1) is valid under the assumption that the external field $\boldsymbol{B}$ is not too large, in such a way that a linear regime is preserved.

As a result, the induced dipole-dipole magnetic force between two beads α and β can be expressed as[18]

$$\boldsymbol{F}^B_{\alpha\beta} = \frac{3\mu_0}{4\pi R^4_{\alpha\beta}} \Big[\left(\boldsymbol{m}_\alpha \cdot \boldsymbol{e}_{\alpha\beta}\right) \boldsymbol{m}_\beta + \left(\boldsymbol{m}_\beta \cdot \boldsymbol{e}_{\alpha\beta}\right) \boldsymbol{m}_\alpha - \left(5\left(\boldsymbol{m}_\beta \cdot \boldsymbol{e}_{\alpha\beta}\right)\left(\boldsymbol{m}_\alpha \cdot \boldsymbol{e}_{\alpha\beta}\right) - \left(\boldsymbol{m}_\alpha \cdot \boldsymbol{m}_\beta\right)\right) \boldsymbol{e}_{\alpha\beta} \Big], \tag{2}$$

where $R_{\alpha\beta} = |\boldsymbol{R}_\alpha - \boldsymbol{R}_\beta|$ is the distance between the beads and $\boldsymbol{e}_{\alpha\beta} = \boldsymbol{R}_{\alpha\beta}/R_{\alpha\beta}$ is the unit vector going from β to α. Finally, in the case of identical solid particles and homogeneous magnetic field $\boldsymbol{B}$, each bead has the same magnetic moment $\boldsymbol{m}_\alpha = \boldsymbol{m}_\beta = \boldsymbol{m}$ and Eq. (2) simplifies to

$$\boldsymbol{F}^B_{\alpha\beta} = \frac{3\mu_0}{4\pi R^4_{\alpha\beta}} \left[2\left(\boldsymbol{m} \cdot \boldsymbol{e}_{\alpha\beta}\right) \boldsymbol{m} - \left(5\left(\boldsymbol{m} \cdot \boldsymbol{e}_{\alpha\beta}\right)^2 - m^2\right) \boldsymbol{e}_{\alpha\beta} \right]. \tag{3}$$

It is convenient to write the magnetic moment as $\boldsymbol{m}_\alpha = m_0(\boldsymbol{B}/B_0)$, where B_0 and $m_0 = \frac{V_c \chi}{\mu_0} B_0$ are, respectively, the characteristic strength of the external field and corresponding magnetic moment. By defining the dimensionless unit vectors $\overline{\boldsymbol{m}} = \boldsymbol{m}/m_0$ and $\overline{R}_{\alpha\beta} = R_{\alpha\beta}/a$, Eq. (3) is rewritten as

$$\boldsymbol{F}^B_{\alpha\beta} = \frac{F_0}{\overline{R}^4_{\alpha\beta}} \left[2\left(\overline{\boldsymbol{m}} \cdot \boldsymbol{e}_{\alpha\beta}\right) \overline{\boldsymbol{m}} - \left(5\left(\overline{\boldsymbol{m}} \cdot \boldsymbol{e}_{\alpha\beta}\right)^2 - 1\right) \boldsymbol{e}_{\alpha\beta} \right], \tag{4}$$

where the characteristic strength of the force is $F_0 = \frac{3\mu_0}{4\pi} \frac{m_0^2}{a^4} = \frac{4\pi}{3\mu_0}(a f \chi B_0)^2$. From Equation (4) the dipole-dipole force can

be split in two components, one parallel (||) to $\boldsymbol{e}_{\alpha\beta}$ and other normal to it (⊥). This reads

$$\boldsymbol{F}^B_{\alpha\beta} = \frac{F_0}{\overline{R}^4_{\alpha\beta}} \Big[\underbrace{2\left(\overline{\boldsymbol{m}}\cdot\boldsymbol{e}_{\alpha\beta}\right)\overline{\boldsymbol{m}}\cdot\left(\boldsymbol{I}-\boldsymbol{e}_{\alpha\beta}\boldsymbol{e}_{\alpha\beta}\right)}_{\perp} + \underbrace{\left(1-3\left(\overline{\boldsymbol{m}}\cdot\boldsymbol{e}_{\alpha\beta}\right)^2\right)\boldsymbol{e}_{\alpha\beta}}_{\parallel}\Big], \tag{5}$$

where $\boldsymbol{I}$ is the identity tensor.

Let us consider now the case of a straight chain forming a small angle θ with the applied rotating magnetic field $\boldsymbol{B}$. Under this condition, the net force calculated from the dipole-dipole force on each bead which is not located at the extremes of the chain will be approximately zero. This can be explained as follows: given that every term from (5) depends on $\boldsymbol{e}_{\alpha\beta}$, the force from the closest neighbor of one bead at one side is almost balanced by the force of the closest neighbor on its other side. Moreover, since the dipole-dipole force scales as $R^{-4}_{\alpha\beta}$, the influence of further neighbors will be negligible. Under this condition, the only beads of the chain undergoing a significant aligning force with the magnetic field are the beads located at the extremes, where the dipole-dipole force is unbalanced and the rotation of the entire chain can be therefore expected to be driven primarily by them. As a consequence, the external beads being driven by the magnetic field will be in advanced positions with respect to the rest of the chain, producing the characteristic S-shape chain deformation *in the direction of rotation* in agreement with previous studies.[12,14,16]

Let us consider now the projection of the force (5) along the center-to-center beads direction $\boldsymbol{e}_{\alpha\beta}$,

$$\begin{aligned}\boldsymbol{F}^B_{\alpha\beta}|_{\boldsymbol{e}_{\alpha\beta}} &= \frac{F_0}{\overline{R}^4_{\alpha\beta}}\left[1-3\left(\overline{\boldsymbol{m}}\cdot\boldsymbol{e}_{\alpha\beta}\right)^2\right]\boldsymbol{e}_{\alpha\beta}\\ &= \frac{F_0}{\overline{R}^4_{\alpha\beta}}\left[1-3\cos^2(\theta)\right]\boldsymbol{e}_{\alpha\beta},\end{aligned} \tag{6}$$

where the second equality comes from the fact that both $\overline{\boldsymbol{m}}$ and $\boldsymbol{e}_{\alpha\beta}$ are unit vectors and θ is the instantaneous angle between $\overline{\boldsymbol{m}}$ (or $\boldsymbol{B}$) and $\boldsymbol{e}_{\alpha\beta}$. Such a force can be attractive as well as repulsive, provided that the angle θ becomes sufficiently large. In particular this will occur when $\arccos\left(1/\sqrt{3}\right) < \theta < \arccos\left(-1/\sqrt{3}\right)$ which can be also written as

$$\left|\frac{\pi}{2}-\theta\right| < \frac{\pi}{2} - \arccos\left(\frac{1}{\sqrt{3}}\right). \tag{7}$$

This value for the critical angle is in agreement with earlier calculations.[9,13] In terms of degrees, such an interval is approximately defined by $|90-\theta| < 35.26$. For angles larger than this value, inter-beads magnetic forces will result in a repulsive (rather than attractive) interaction.

The rotating chain is therefore under the influence of a dissipative torque which is opposite to the magnetic torque aligning the chain to the magnetic field. If at some instant, the strength of the magnetic torque is able to compensate the viscous one, the chain will remain in a stable configuration. In the opposite case, the phase lag between the chain and the magnetic field will eventually not satisfy Eq. (7) and the repulsion force will break the chain. Given the S-shape of the chain this will happen first in the center of the chain, which is the most delayed region in terms of alignment with the external field. This is also the reason for the typical chain's rupture at its center (see Sec. IV A).

1. Concluding scenario

When the magnetic field is rotating, the alignment of the chain is delayed with respect to the magnetic field direction by the presence of the surrounding viscous fluid.

(i) If the frequency of rotation is relatively small (in a sense to be discussed later), the chain will follow the magnetic field in a quasi-straight shape, i.e., for small angles θ only a negligible deflection in the last beads of the chain will occur.
(ii) If the frequency of rotation becomes higher, significant deflection of the beads at the end of the chain will trigger deflection within the chain delivering the final visible S-shape.
(iii) The angle of two-consecutive beads is different along the S-shaped chain. Given that the beads located at the extremes are the ones which drive the chain alignment with the magnetic field, the greater differences between the angle θ of the magnetic field and the chain will be exactly in the middle of the chain. If the frequency becomes sufficiently high, the chain cannot follow the magnetic field, and the angle θ in the middle of the chain will be eventually in the range (7). Under this condition, only the beads in that central region will feel a repulsive magnetic force and the chain will suddenly breakup.

B. Critical chain's breakup frequency

In this section, the model discussed above is analyzed. An analytical expression for the chain's breakup frequency is provided, which will be compared against full three-dimensional SPH direct numerical simulations in Sec. IV and with the experimental data in Sec. V.

1. 0th-order drag approach

It is clear that if the extremal beads are able to follow the magnetic field closely (i.e., without delay), no chain breaking will take place. The magnitude of the solvent viscosity is a key parameter in the determination of this condition. The typical S-shape of the chain is also an effect of the viscosity, which is indirectly responsible of the resistance of the central particles of the chain in following the movement of the extreme ones.

To simplify the problem and to obtain an analytical expression for the breakup frequency, the chain is considered, in first approximation, straight. Given that the rotation of the chain is driven mainly by the external beads, it will be considered that all the magnetic torque is exerted by those beads. Once the external beads have moved, the remaining internal beads follow the external ones due to the magnetic attraction force between the beads. The magnetic force on an external bead (e.g., $\alpha = N$) is given by Equation (4). The typical torque applied by the magnetic field can be calculated as

$$\boldsymbol{\tau}^B = L\boldsymbol{e}_c \times \boldsymbol{F}^B_N, \tag{8}$$

where, being the chain straight, the indices α and β have been omitted (i.e., $\boldsymbol{e}_{\alpha\beta} = \boldsymbol{e}_c$ is the constant unit vector defining the chain direction) and $\boldsymbol{F}_N^B$ is the force exerted on one extreme bead given by (4). Finally, L is the chain length which can be estimated as (center-to-center distance between the extreme particles)

$$L = (N-1)d, \tag{9}$$

where N is the total number of beads of the chain and d is the characteristic center-to-center distance between the adjacent beads.

Let us consider now the case of a chain rotating with an angular velocity ω' under the influence of a field $\boldsymbol{B}$ which is rotating with an angular velocity ω. If it is supposed that the only important magnetic interaction on the external beads is due to the influence of their closest neighbors, the force on the external beads due to the magnetic field can be calculated as

$$\boldsymbol{F}_N^B = \frac{F_0}{\overline{d}^4}\left[2\left(\overline{\boldsymbol{m}}\cdot\boldsymbol{e}_c\right)\overline{\boldsymbol{m}} - \left(5(\overline{\boldsymbol{m}}\cdot\boldsymbol{e}_c)^2 - 1\right)\boldsymbol{e}_c\right], \tag{10}$$

where $\overline{d} = d/a$ is the dimensionless characteristic distance between adjacent beads, and

$$\begin{aligned}\overline{\boldsymbol{m}} &= (\cos(\omega t+\phi),\ 0,\ \sin(\omega t+\phi)),\\ \boldsymbol{e}_c &= (\cos(\omega' t+\phi'),\ 0,\ \sin(\omega' t+\phi')),\end{aligned} \tag{11}$$

being ϕ and ϕ', respectively, the initial phases of the rotation of the magnetic field and the chain direction. Note that the x–z plane has been defined as the rotation plane. The magnetic torque is given then by

$$\boldsymbol{\tau}^B = -2L\frac{F_0}{\overline{d}^4}\left(\overline{\boldsymbol{m}}\cdot\boldsymbol{e}_c\right)\left(\overline{\boldsymbol{m}}\times\boldsymbol{e}_c\right). \tag{12}$$

The dot and cross products are calculated as

$$\begin{aligned}\overline{\boldsymbol{m}}\cdot\boldsymbol{e}_c &= \cos\left((\omega-\omega')t + (\phi-\phi')\right),\\ \overline{\boldsymbol{m}}\times\boldsymbol{e}_c &= \left(0,\ -\sin\left((\omega-\omega')t+(\phi-\phi')\right),\ 0\right).\end{aligned} \tag{13}$$

Now, the application of the friction torque on the chain is going to be considered. The expression for the friction torque in the shish-kebab model presented in Ref. 19 has been used before.[9,12,14] In that expression, valid for long chains ($N >> 1$), the translational drag force of the particles and hydrodynamic interactions between them are considered. In order to make that expression valid for smaller chains, in Ref. 20 they assimilate the chain of particles to a prolate ellipsoid, and propose a phenomenological law which is fitted through the experimental data. Such an expression was also used in Ref. 16. In our case, the friction on the particle α is given by the Stoke's Law

$$\boldsymbol{F}_\alpha^\nu = -6\pi\eta a\boldsymbol{\omega}'\times\boldsymbol{R}_\alpha \tag{14}$$

and by the rotational friction

$$\boldsymbol{\tau}_\alpha^R = -8\pi\eta a^3\boldsymbol{\omega}', \tag{15}$$

so the total torque on the chain due to the solvent viscosity reads

$$\begin{aligned}\boldsymbol{\tau}^\nu &= -6\pi\eta a\sum_\alpha \boldsymbol{R}_\alpha\times(\boldsymbol{\omega}'\times\boldsymbol{R}_\alpha)\\ &\quad+\sum_\alpha\boldsymbol{\tau}_\alpha^R = -2\pi\eta a\boldsymbol{\omega}'\left[3\sum_\alpha R_\alpha^2 + 4a^2N\right],\end{aligned} \tag{16}$$

where the expression of the double cross product has been used and the origin of coordinates has been located in the middle of the chain, so $\boldsymbol{R}_\alpha$ and $\boldsymbol{\omega}'$ are normal. The evolution of the rotation dynamics can be written now as

$$I\frac{d\boldsymbol{\omega}'}{dt} = \boldsymbol{\tau}^B + \boldsymbol{\tau}^\nu, \tag{17}$$

or by using (12), (13), and (16)

$$\begin{aligned}I\frac{d\omega'}{dt} &= L\frac{F_0}{\overline{d}^4}\sin\left(2(\omega-\omega')t+2\phi_0\right)\\ &\quad-2\pi\eta a\omega'\left[3\sum_\alpha R_\alpha^2 + 4a^2N\right],\end{aligned} \tag{18}$$

where I is the moment of inertia of the chain and $\phi_0 = \phi - \phi'$. By assuming that a stationary state can be established in such a way that the chain is able to follow the magnetic field (i.e., $\omega' = \omega$), the equation reads

$$0 = L\frac{F_0}{\overline{d}^4}\sin(2\phi_0) - 2\pi\eta a\omega\left[3\sum_\alpha R_\alpha^2 + 4a^2N\right]. \tag{19}$$

From this equation, the equilibrium change of phase ϕ_0 can be obtained as

$$\sin(2\phi_0) = \frac{2\pi\eta\omega a^2}{F_0}\left(\frac{N}{N-1}\right)\overline{d}^3\left(\frac{1}{4}\left(N^2-1\right)\overline{d}^2+4\right), \tag{20}$$

where it has been taken into account that $\sum_\alpha R_\alpha^2 = \frac{1}{12}N(N^2-1)d^2$ and we have used Eq. (9).

As long as the maximum magnetic torque (given at $\phi_0 = \pi/4$) is greater than the total viscous torque, the chain will remain in a stable configuration following steadily the rotating field. On contrary, if the angle $\phi_0 > \pi/4$, the maximum magnetic torque will not be able to balance the viscous torque. Under this condition, the angles ϕ_0 obtained under the steady assumption in Eq. (20) will represent an unstable solution and the chain will increasingly delay with respect to the external field until the breaking angle $\theta_c = \arccos\left(\pm 1/\sqrt{3}\right)$, given by Eq. (7), is reached. At that precise moment, the transition from attractive to repulsive magnetic interaction will trigger the final chain rupture.

In conclusion, in order to prevent chain breakup, ϕ_0 should remain always below $\pi/4$. This allows us to define a critical frequency ω_c for which the chain destabilizes

$$\omega_c = \frac{F_0}{2\pi\eta a^2}\left(\frac{N-1}{N}\right)\overline{d}^{-3}\left(\frac{1}{4}\left(N^2-1\right)\overline{d}^2+4\right)^{-1}, \tag{21}$$

For frequencies larger than ω_c, no steady phase shift can be established, the chain will not be able to follow the external magnetic field as a whole, and destabilization leading to final breakup will start.

2. High-order lubrication approach

In the problem of chaining, adjacent particles might get very close to each other, i.e., at surface-to-surface distances much smaller than their radius. Under this condition, the overall viscous dissipation from the fluid manifests, beside through the Stoke's and rotational drags on single beads, also via lubrication interactions between the adjacent beads. It should be remarked that for very close beads, this force can be orders

of magnitude larger than to the Stoke's drag[17] and therefore it is crucial to take into account this effect for a quantitative decryption of the problem.

Again, we will consider a straight chain. The distance between particles is assumed not changing significantly (i.e., before breakup), in such a way that normal lubrication would not be important. On the other hand, since the movement of the chain is rotatory, tangential velocities of different beads will be different (i.e., increasing towards the extremes) and therefore tangential lubrication will be important. Furthermore, it is considered that the net effect of such a lubrication force will be relevant only for the extreme beads of the chain, given that for the internal ones such lubrication forces will be balanced from by two neighbors at each side of the given bead.

If α is an extreme bead (i.e., N), the overall tangential lubrication force that feels from its unique neighbor $N-1$ reads[21]

$$\begin{aligned} \boldsymbol{F}_N^{\mathrm{lub},t} &= -\pi\eta a \ln\left(\frac{a}{d-2a}\right)(\boldsymbol{V}_N - \boldsymbol{V}_{N-1}) \\ &= -\pi\eta a d \ln\left(\frac{a}{d-2a}\right)\boldsymbol{\omega}' \times \boldsymbol{e}_c, \end{aligned} \tag{22}$$

so that the total torque due to the tangential lubrication force is given by

$$\begin{aligned} \boldsymbol{\tau}^{\mathrm{lub},t} \approx \boldsymbol{\tau}_N^{\mathrm{lub},t} &= -\pi\eta a d \ln\left(\frac{a}{d-2a}\right)\boldsymbol{R}_N \times (\boldsymbol{\omega}' \times \boldsymbol{e}_c) \\ &= -\pi\eta a d^2 (N-1) \ln\left(\frac{a}{d-2a}\right)\boldsymbol{\omega}', \end{aligned} \tag{23}$$

where $R_N = L/2 = (N-1)d/2$, given that $\alpha = N$ is an extreme particle. Note also that there are two extremes ($\alpha = 1, N$), so the overall torque must be doubled. The equation of evolution of the dynamics of the chain (17) is therefore modified by an additional lubrication term and reads now

$$I\frac{d\boldsymbol{\omega}'}{dt} = \boldsymbol{\tau}^B + \boldsymbol{\tau}^\nu + \boldsymbol{\tau}^{\mathrm{lub},t} = -2L\frac{F_0}{\overline{d}^4}(\overline{\boldsymbol{m}} \cdot \boldsymbol{e}_c)(\overline{\boldsymbol{m}} \times \boldsymbol{e}_c) - C\boldsymbol{\omega}', \tag{24}$$

where

$$\begin{aligned} C &= 6\pi\eta a \sum_\alpha R_\alpha^2 + 8\pi\eta a^3 N + \pi\eta a d^2 (N-1)\ln\left(\frac{a}{d-2a}\right) \\ &= \pi\eta a^3\left(\frac{1}{2}N\left(N^2-1\right)\overline{d}^2 + 8N + \overline{d}^2(N-1)\ln\left(\frac{1}{\overline{d}-2}\right)\right). \end{aligned} \tag{25}$$

By following the same steps than in Section II B 1, the next expression is found

$$\omega_c = \frac{(N-1)F_0 a^4}{d^3 C}, \tag{26}$$

or by replacing (25)

$$\begin{aligned} \omega_c = \frac{F_0}{\pi\eta a^2}\frac{(N-1)}{\overline{d}^3}\Bigg(&\frac{1}{2}N\left(N^2-1\right)\overline{d}^2 \\ &+ 8N + \overline{d}^2(N-1)\ln\left(\frac{1}{\overline{d}-2}\right)\Bigg)^{-1}. \end{aligned} \tag{27}$$

Note that for N high enough, only the drag Stoke's term, which scales as $\sim N^3$, is important. So tangential lubrication and rotational drag force are important only for small chains. Note that the same scaling $\omega_c \sim 1/N^2$ for long chains calculated in the Franke *et al.* work[15] is found here. This differs slightly from the scaling $\log(N)/N^2$ obtained in other works.[13,14,16]

III. SPH MODEL OF SUSPENDED MAGNETIC BEADS

In this section, the details of the SPH simulation method, used to validate our theory, are presented, separately, for the solvent medium, the suspended solid particles and magnetic interactions.

A. Suspending Newtonian fluid

SPH is a meshless Lagrangian fluid model where the Navier-Stokes equations describing a Newtonian liquid are discretized using a set of points denoted as fluid particles. Positions and momenta of every fluid particle (labelled by Latin indices $i = 1, \cdots, N_{SPH}$) evolve in a Lagrangian framework, according to the SPH discrete equations.[22]

$$\dot{\boldsymbol{r}}_i = \boldsymbol{v}_i, \tag{28}$$

$$\begin{aligned} m\dot{\boldsymbol{v}}_i = &-\sum_j\left[\frac{P_i}{d_i^2} + \frac{P_j}{d_j^2}\right]\frac{\partial W(r_{ij})}{\partial r_{ij}}\boldsymbol{e}_{ij} \\ &+ \sum_j (D+2)\eta_0\left[\frac{1}{d_i^2} + \frac{1}{d_j^2}\right]\frac{\partial W(r_{ij})}{\partial r_{ij}}\frac{\boldsymbol{e}_{ij}\cdot\boldsymbol{v}_{ij}}{r_{ij}}\boldsymbol{e}_{ij}, \end{aligned}$$

where D is the number of dimensions of the system, P_i the pressure of particle i, $\boldsymbol{e}_{ij} = \boldsymbol{r}_{ij}/r_{ij}$ the unit vector joining particles i and j, $\boldsymbol{v}_{ij} = \boldsymbol{v}_i - \boldsymbol{v}_j$ their velocity difference, and η_0 the viscosity of the solvent. $d_i = \sum_j W(r_{ij}, r_{cut})$ is the number density associated to the particle i estimated as a weighted interpolation with a bell-shaped function W with compact support r_{cut}.[23] With this definition, mass conservation and continuity equations for the mass density $\rho_i = md_i$ (m particle mass) are implicitly satisfied, whereas the Newton's equations of motion (28) for the particles are a discrete representation of the momentum Navier-Stokes equation in a Lagrangian framework, with the first summation in Eq. (28) representing the pressure gradient term and second summation corresponding to the Laplacian of the velocity field. For the weighting function W, the present work adopts a quintic spline kernel[24] with a cutoff radius $r_{cut} = 3\,dx$ (dx being the mean fluid particle separation).[25] Finally, an equation of state for the pressure is used relating it to the estimated local mass density, i.e., $P_i = p_0[(\rho_i/\rho_0)^\gamma - 1] + p_b$, where the input parameters ρ_0, p_0 and γ are chosen to have a liquid speed of sound $c_s = \sqrt{\gamma p_0/\rho_0}$ sufficiently larger than any other velocity present in the problem, therefore enforcing approximate incompressibility[26] and p_b is a background pressure.

B. Solid particles: Fluid-structure interaction

Solid inclusions of arbitrary shape can be modelled using boundary particles similar to the fluid ones, located inside the solid region.[27] Boundary particles interact with the fluid particles by means of the same SPH forces described in Eq. (28). No-slip boundary condition at the liquid-solid interface is enforced during each interaction between the fluid particle i and boundary particle j by assigning an artificial

velocity to the boundary particle j, which satisfy zero interpolation at the interface.[24] The same approach can be also used to model any arbitrary external wall. Once all the forces acting on every boundary particle j belonging to a solid bead (labelled by Greek indexes α) are calculated, the total force $\boldsymbol{F}_\alpha^{\text{sph}}$ and torque $\boldsymbol{T}_\alpha^{\text{sph}}$ exerted by the surrounding fluid modelled by SPH can be obtained as

$$\begin{aligned} \boldsymbol{F}_\alpha^{\text{sph}} &= \sum_{j\in\alpha} \boldsymbol{F}_j \\ \boldsymbol{T}_\alpha^{\text{sph}} &= \sum_{j\in\alpha} \left(\boldsymbol{r}_j - \boldsymbol{R}_\alpha\right) \times \boldsymbol{F}_j, \end{aligned} \tag{29}$$

where $\boldsymbol{R}_\alpha$ is the center of mass of the solid bead α. When properly integrated, $\boldsymbol{F}_\alpha^{\text{sph}}$ and $\boldsymbol{T}_\alpha^{\text{sph}}$ allow to obtain the new linear velocity $\boldsymbol{V}_\alpha$, angular velocity $\boldsymbol{\Omega}_\alpha$, and position of the suspended solid bead. Positions of boundary particles inside α are finally updated according to a rigid body motion.[28] In the following, we assume that $\alpha = 1, \ldots, N$, where N is the total number of solid beads.

C. Interparticle lubrication/repulsion/magnetic forces

The present SPH model captures accurately the long range hydrodynamic interactions (HIs) between solid particles.[27] As discussed in detail in Refs. 17, 28, and 29, when two solid particles (e.g., α and β) get very close to each other, the HIs mediated by the SPH fluid are poorly represented and need to be corrected. In Refs. 17, 28, and 29, an analytical solution has been considered for the pairwise short-range HIs obtained in the limit of small sphere's separation and superimposed it to the far-field multi-body SPH HIs. The normal and tangential lubrication forces acting between the spheres read[21]

$$\begin{aligned} \boldsymbol{F}_{\alpha\beta}^{\text{lub},n}(s) &= f_{\alpha\beta}(s)\boldsymbol{V}_{\alpha\beta} \cdot \boldsymbol{e}_{\alpha\beta}\boldsymbol{e}_{\alpha\beta}, \\ \boldsymbol{F}_{\alpha\beta}^{\text{lub},t}(s) &= g_{\alpha\beta}(s)\boldsymbol{V}_{\alpha\beta} \cdot \left(\boldsymbol{1} - \boldsymbol{e}_{\alpha\beta}\boldsymbol{e}_{\alpha\beta}\right), \end{aligned} \tag{30}$$

where $\boldsymbol{e}_{\alpha\beta} = \boldsymbol{R}_{\alpha\beta}/R_{\alpha\beta}$ is the vector joining the centers of mass of solid particles α and β, $\boldsymbol{V}_{\alpha\beta}$ is their relative velocity, and $s = R_{\alpha\beta} - (a_\alpha + a_\beta)$ is the distance in the gap between sphere-sphere surfaces. Here, the scalar functions $f_{\alpha\beta}(s)$ and $g_{\alpha\beta}(s)$ are defined as

$$\begin{aligned} f_{\alpha\beta}(s) &= -6\pi\eta \left[\left(\frac{a_\alpha a_\beta}{a_\alpha + a_\beta}\right)^2 \frac{1}{s} + a_\alpha \left(\frac{1 + 7\frac{a_\beta}{a_\alpha} + \left(\frac{a_\beta}{a_\alpha}\right)^2}{5\left(1 + \frac{a_\beta}{a_\alpha}\right)^3}\right) \right. \\ &\quad \left. \times \ln\left(\frac{a_\alpha}{s}\right)\right], \\ g_{\alpha\beta}(s) &= -6\pi\eta a_\alpha \left[\frac{4\frac{a_\beta}{a_\alpha}\left(2 + \frac{a_\beta}{a_\alpha} + 2\left(\frac{a_\beta}{a_\alpha}\right)^2\right)}{15\left(1 + \frac{a_\beta}{a_\alpha}\right)^3}\right] \ln\left(\frac{a_\alpha}{s}\right), \end{aligned} \tag{31}$$

where a_α and a_β are the sphere's radii. As discussed in Refs. 17, 28, and 29, excellent agreement is obtained in the description of HIs over the entire range of interparticle distances s. An accurate semi-implicit splitting scheme[30] for the time integration of the short-range lubrication forces presented in Ref. 29 is used.

Beside lubrication forces, an additional short-range repulsive force acting between solid particles is introduced to mimic particle's surface roughness or other short-range interactions (e.g., electrostatic) which prevents overlap. It is customary to use for this force the expression,[31,32]

$$\boldsymbol{F}_{\alpha\beta}^{\text{rep}} = F^{\text{rep}} \frac{\tau e^{-\tau s}}{1 - e^{-\tau s}} \boldsymbol{e}_{\alpha\beta}, \tag{32}$$

where τ^{-1} determines the interaction range and F^{rep} its magnitude. In this work, $\tau^{-1} = 0.001a$ and $F^{rep} = 0.02115$ are adopted, corresponding to a nearly hard-sphere model.

Finally, the interparticle magnetic interaction is also considered and calculated via Eq. (5). Note that under typical conditions, the magnetic field strength in Eq. (5) is quite large and exceeds the thermal energy of the bead significantly. Similarly as in the experiments by Franke *et al.*,[15] in our simulation we choose a ratio between the magnetic and the thermal energies given by $\lambda = W_m/k_BT = \mu_0 m_0^2/(16\pi a^3 k_B T) \sim 1000$ so that Brownian motion should have a negligible effect on the chain dynamics.[3] For very weak magnetic fields, Brownian effects can be however relevant and they could be easily incorporated in our formalism by considering the stochastic generalization of the SPH equations given in (28), i.e., the smoothed dissipative particle dynamics method for a thermal solvent.[27,33]

IV. NUMERICAL RESULTS

In this section, the analytical results obtained in Sec. II for the dynamics, deformation, and breakup of a rotating chain are compared with the full three-dimensional direct numerical simulations using the SPH model discussed in Sec. III. Chains composed of different numbers of magnetic beads N ranging from 4 to 11 are considered. The beads have constant radius $a = 1$ and are modelled with approximately 120 SPH frozen particles. The simulation box is chosen as $L_x \times L_y \times L_z = 50 \times 25 \times 50$ in radius units, corresponding to a total number of SPH particles $N_{SPH} = 1\,600\,000$. The mean SPH particle distance is $\Delta x = 0.33$. This size of the simulation box rules out finite size effects resulting from the application of periodic boundary conditions. The characteristic strength of the dipole-dipole force is $F_0 = 1.63$. The suspending medium is Newtonian, characterized by a viscosity $\eta_0 = 0.2$ and the speed of sound $c_S = 2.0$ is chosen to be much larger than the maximal linear rotational velocity of the chain. The resulting Reynolds number is always smaller than 0.1, based on the maximal bead velocity. A rotating external magnetic field is considered $\boldsymbol{B} = B_0(\cos(\omega t), 0, \sin(\omega t))$. The combined effect of chain length L, magnetic strength B_0, solvent viscosity η_0, and rotation frequency ω on the corresponding chain's dynamics is explored and compared with the numerical results.

A. Chain dynamics: Deformation and breakup

In Figure 2 (Multimedia view) snapshots corresponding to three typical scenarios are depicted: (i) For a small frequency ($\omega \ll \omega_c$) (Fig. 2 left (Multimedia view)), the magnetic chain follows closely and steadily the applied external magnetic field; the chain rotates as a quasi-rigid rod with small deformations visible only at its ends. (ii) At moderate frequencies ($\omega < \omega_c$) (Fig. 2 center (Multimedia view)), the steady phase-shift between the chain and magnetic field increases,

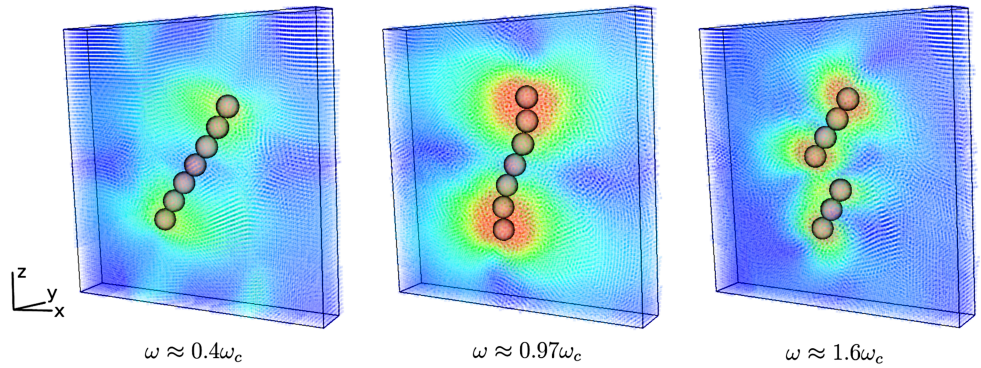

FIG. 2. Snapshots of simulations. The small points represent the fluid particles which have a palette of colors depending of their velocity (red is faster and blue slower). In order to have a clearer view of the chain, only the slice containing it has been drawn. (Multimedia view) [URL: http://dx.doi.org/10.1063/1.4978630.1] [URL: http://dx.doi.org/10.1063/1.4978630.2] [URL: http://dx.doi.org/10.1063/1.4978630.3]

producing a visible S-shape deformation in the rotation direction. (iii) For a sufficiently large frequency ($\omega > \omega_c$) (Fig. 2 right (Multimedia view)), the phase-shift in the central part of the chain grows and exceeds eventually the critical angle for the onset of repulsion effects where breakup occur. For a detailed movie of the three cases, the reader is referred to Fig. 2 (Multimedia view).

In Figure 3 the angle θ of the central bead of a chain made by 7 beads with its closest neighbors has been drawn for four different frequencies. The points have been drawn only when the chain is not broken (so angle θ can be defined). It is considered that the chain is broken or in process of breaking when the distance between the two adjacent beads surfaces becomes twice or larger than their value at equilibrium. In all the cases, the inputs of the simulations are the same as discussed above; the external field frequency varies between $0.4\omega_c$ and $3.2\omega_c$. The shift angle is compared with the critical angle $\theta_c = \arccos\left(\pm\frac{1}{\sqrt{3}}\right)$, given by Equation (7) and represented in the figure by the solid black line. The black dashed line represents the angle $\pi/4$, which determines the stability

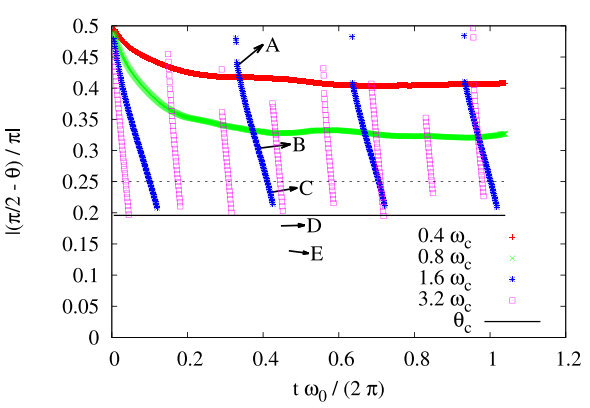

FIG. 3. Angle of the central bead of a chain of 7 particles with its closest neighbors. Such an angle is compared with the critical angle θ_c defined by the equality limit of (7). The black dashed line represents the angle $\pi/4$. It is not possible for an equilibrium lag phase below that line. The points have been drawn only when the chain is not broken. All of the simulations have the same parameters but the frequency. Frames at points A, B, C, D, and E of the simulation for $\omega = 2\omega_0$ have been drawn at Figure 4. Note that the points of the curve at D and E have not been drawn because the chain is broken there.

of the chain: if the phase lag in the figure goes beyond that line, the chain will reach the angle θ_c and will break up. In the cases when the chain does not break (i.e., the two smallest frequencies corresponding to red/green lines), the typical angles between the center of the chain and the magnetic field do never approach θ_c. Moreover, they reach an equilibrium value which indicates that the chain is able to steadily follow the rotation of the magnetic field, although with a constant finite delay. On the other hand, in the rest of the cases (i.e., two highest frequencies, blue/pink lines) the chain breaks several times during the simulation. This event happens exactly at those instants when the angle between the chain and the magnetic field approaches the value θ_c. As already explained, this is due to the fact that the chain is not able to rotate fast enough to match the angular velocity of the magnetic field leading to an increasing shift. After a certain time, the delay becomes sufficiently large such that the force between the beads in the center of the chain turns into repulsive, initiating the rupture process. After that, the resulting chains, which are smaller, are able to follow the rotation of the magnetic field. After half complete rotation, the extremes of the chains, they re-attach starting the process again and generating the characteristic periodic behavior observed in Figure 3.

To better visualize the breakup process, in Figure 4 several configurations of the chain have been drawn for an applied frequency $\omega = 1.6\omega_c$ (corresponding to the blue points A-E in Fig. 3 and to the third scenario in Fig. 2 (Multimedia view)). The magnetic field orientation at different times of the simulation is depicted as a dashed blue line, whereas the red circles represent the positions of the beads (the size of the circles does not correspond to the size of the beads). It is clear that the largest difference between the orientation of the magnetic field and single bead alignment takes place in the middle of the chain. Shadowed areas represent the regions characterized by local angles with respect to **B**, $\theta > \theta_c$. For central bead orientations within these regions, the magnetic interparticle force becomes repulsive. Note frame C where the chain is still uncut and its central orientation does overlap quasi with the border of the shadowed repulsive region. For configuration D, such an angle is beyond θ_c and breakup initiates. The chain is completely broken at configuration E, where the smaller chains independently follow the rotation of the magnetic field.

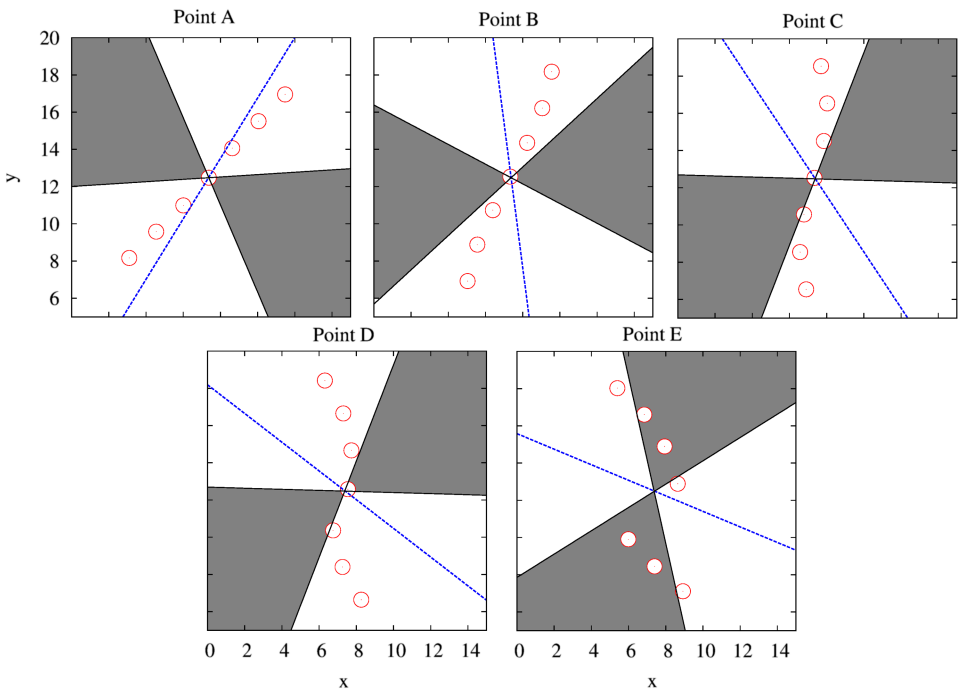

FIG. 4. Frames of the times A, B, C, D, and E indicated at Figure 3 from the simulation with $\omega = 2\omega_0$. The blue dashed-line is the orientation of the magnetic field and the red circles are the centers of the beads of the chain. Shadowed areas have been drawn when the chain is not broken, which correspond to the areas where the force between the central beads would be repulsive if the magnetic field orientation would lay inside it. The size of the circles does not correspond to the size of the beads.

B. Critical breakup frequency

In this section, the critical breakup frequency obtained from three-dimensional SPH simulations of the magnetic model discussed in Sec. III is compared quantitatively with the analytical predictions of Sec. II B and previous theoretical results. For sake of simplicity, the equations will be expressed in terms of the magnetization M, which is related with F_0 as $F_0 = \frac{4\pi}{3}\mu_0 M^2 a^2$.

In Fig. 5, ω_c vs N (number of beads forming the chain) is shown for the next cases:

- Circles with error bars represent the results of SPH simulations. Note that error bars are smaller than the size of the circles.
- Blue line is the critical frequency calculated in Ref. 15 by Franke *et al.*, i.e.,

$$\omega_c^A = \frac{1}{9}\frac{\mu_0 M^2}{\eta}\frac{1}{N^2}, \tag{33}$$

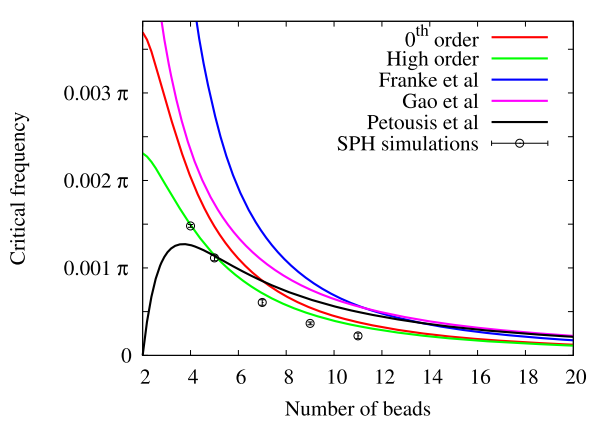

FIG. 5. Simulation results (circles with error bars) compared with our model (red and green lines) and Franke *et al.* (blue line), Gao *et al.* (pink line), and Petousis *et al.* (black line) models.

where $M = m_0/V$ is the magnetization.

- In Gao *et al.*[16] a dimensionless number R_T is defined which represents the ratio between the viscous drag and the maximum magnetic driven torque. The chain breaks up when $R_T = 1$, which allows us to define the next critical frequency

$$\omega_c^B = \frac{1}{16}\frac{\mu_0 M^2}{\eta}\frac{(N-1)\left(\log(N/2) + \frac{2.4}{N}\right)}{N^3}. \tag{34}$$

Such a frequency has been drawn as a purple line.

- By using the magnetic and viscous torques proposed by Petousis *et al.*[14] and following the procedure described in this work, the critical frequency of the chain can be calculated (black line), which is given by

$$\omega_c^C = \frac{1}{16}\frac{\mu_0 M^2}{\eta}\frac{(N-1)\log(N/2)}{N^3}. \tag{35}$$

- By considering in our 0-th order drag result (Eq. (21)), a distance between the beads of the chain exactly equal to their diameter (i.e., $d = d_0 = 2a$), i.e., touching beads, the analogous result is obtained (red line)

$$\omega_c^{0\text{-th}} = \frac{1}{12}\frac{\mu_0 M^2}{\eta}\frac{N-1}{N\left(N^2+3\right)}. \tag{36}$$

- The higher-order lubrication formula (Eq. (27)), which is also rewritten here for clarity

$$\omega_c^{\text{high}} = \frac{4}{3}\frac{\mu_0 M^2}{\eta}\frac{(N-1)}{\bar{d}^3}\left(\frac{1}{2}N\left(N^2-1\right)\bar{d}^2 + 8N + \bar{d}^2(N-1)\ln\left(\frac{1}{\bar{d}-2}\right)\right)^{-1}, \tag{37}$$

is depicted as green line in Fig. 5.

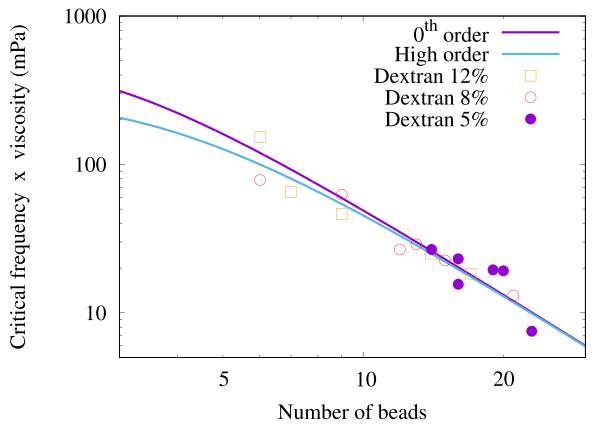

FIG. 6. Presented models with $f = 0.65$ compared to the experimental data from Ref. 15. The squares and circles show the experimental data obtained at different viscosities (dextran concentration).

It is clear that the drag-based approximations (both Franke *et al.*, Gao *et al.* and our 0th-*order* model) reproduce qualitatively the decrease of ω_c for increasing chain length, but they quantitatively overpredict the critical breakup frequencies, especially for small chains. On contrary, the lubrication-based solution (high-order) is able to match fairly well the simulation data, especially for $N < 9$.

Note that in the theoretical derivations, we still rely on the assumption that the chain is straight. For larger chains, of course this approximation becomes increasingly rude. In particular, for real deformed chains, the change of phase between the magnetic field and the center of the chain will be obviously greater than the one corresponding to an approximate straight rigid chain, and the critical breakup frequency ω_c is expected to be smaller than the one estimated here. This can explain the smaller frequency obtained in the real SPH simulation data (black circles) with respect to analytical expression (27) for $N \geq 9$.

V. COMPARISON WITH EXPERIMENTS

In Sec. IV B it has been shown that under controlled conditions, i.e., when all parameters are known, the agreement of the new high-order model including lubrication effects with the simulations is excellent. In this section, the results of the model are compared with the experimental data presented in Ref. 15. According to experimental conditions: $B_0 = 15$ mT, $a = 0.5$ μm, and $\chi = 1.4$. For a spherical bead, its effective magnetic susceptibility can be written as Ref. 16 $\chi_p = \chi/(1+\chi/3)$. The only parameter which remains undetermined in experiments is the value of the paramagnetic fraction $f \in [0, 1]$ of the bead's volume which will be used next as a fitting parameter. In Figure 6 our model is compared with the experimental data for several dextran solutions of different viscosities: best fitted value gives $f = 0.65$. Whereas both models capture the general scaling of the experimental data equally well, difference between them takes place for small-size chains. Scattering in experimental data does not allow to discriminate clearly between the two lines; however, we point out that simulation results (see Fig. 5 in linear scale) suggest that the high-order lubrication model can better capture this regime.

VI. CONCLUSIONS

In this paper, a model of linear chain of superparamagnetic beads has been presented in order to describe its dynamics and to calculate the critical frequency for instability under an applied rotational magnetic field. As in Ref. 16 we have considered that the relevant mechanism aligning the chain to the magnetic field orientation is the induced dipole-dipole forces of the external beads. On the other hand, the viscous torque on the chain induces a delay in the alignment. With these assumptions, the S-shape deformation of the chain can be qualitatively understood. Two different straight chain models have been proposed: in the first one, the friction torque is uniquely based on the translational and rotational drags of the particles of the chain; in the second one, additional lubrication forces between particles are considered. With these models it is possible to determine an expression for the critical frequency which is able to capture quantitatively the chain breakup. To test our model under controlled conditions, we have performed direct numerical simulations using the SPH method. Excellent agreement with our model is found, especially for small chain size. The proposed models have been also compared with the experimental data presented by Franke *et al.*[15] and are in excellent agreement for a paramagnetic fraction f of 65%.

ACKNOWLEDGMENTS

The Authors gratefully acknowledge the financial support provided by the Welsh Government and Higher Education Funding Council for Wales through the Ser Cymru National Research Network in Advanced Engineering and Materials. Computing resources offered by HPC Wales via the Project No. HPCWT050 (Multiscale particle simulation for complex fluids) is also gratefully acknowledged.

[1] A. S. Silva, R. Bond, F. Plourabouné, and D. Wirtz, "Fluctuation dynamics of a single magnetic chain," Phys. Rev. E **54**, 5502 (1996).
[2] S. Cutillas, G. Bossis, and A. Cebers, "Flow-induced transition from cylindrical to layered patterns in magnetorheological suspensions," Phys. Rev. E **57**, 804 (1998).
[3] S. Melle, O. G. Calderón, M. A. Rubio, and G. G. Fuller, "Rotational dynamics in dipolar colloidal suspensions: Video microscopy experiments and simulations results," J. Non-Newtonian Fluid Mech. **102**, 135–148 (2002).
[4] S. Melle, O. G. Calderón, M. A. Rubio, and G. G. Fuller, "Microstructure evolution in magnetorheological suspensions governed by mason number," Phys. Rev. E **68**, 041503 (2003).
[5] A. K. Vuppu, A. A. Garcia, and M. A. Hayes, "Video microscopy of dynamically aggregated paramagnetic particle chains in an applied rotating magnetic field," Langmuir **19**, 8646–8653 (2003).
[6] S. L. Biswal and A. P. Gast, "Rotational dynamics of semiflexible paramagnetic particle chains," Phys. Rev. E **69**, 041406 (2004).
[7] Y. Hwang and X. Wu, "Quasi-two-dimensional domain structures of magnetic particles in a static field," Phys. Rev. E **49**, 3102 (1994).
[8] J. Liu, E. Lawrence, A. Wu, M. Ivey, G. Flores, K. Javier, J. Bibette, and J. Richard, "Field-induced structures in ferrofluid emulsions," Phys. Rev. Lett. **74**, 2828 (1995).
[9] S. Melle, G. G. Fuller, and M. A. Rubio, "Structure and dynamics of magnetorheological fluids in rotating magnetic fields," Phys. Rev. E **61**, 4111 (2000).
[10] S. Melle, O. G. Calderón, G. G. Fuller, and M. A. Rubio, "Polarizable particle aggregation under rotating magnetic fields using scattering dichroism," J. Colloid Interface Sci. **247**, 200–209 (2002).
[11] S. Melle, O. G. Calderón, M. A. Rubio, and G. G. Fuller, "Chain rotational dynamics in mr suspensions," Int. J. Mod. Phys. **16**, 2293–2299 (2002).
[12] S. Melle and J. E. Martin, "Chain model of a magnetorheological suspension in a rotating field," J. Chem. Phys. **118**, 9875–9881 (2003).

[13] A. Cēbers and I. Javaitis, "Dynamics of a flexible magnetic chain in a rotating magnetic field," Phys. Rev. E **69**, 021404 (2004).
[14] I. Petousis, E. Homburg, R. Derks, and A. Dietzel, "Transient behaviour of magnetic micro-bead chains rotating in a fluid by external fields," Lab Chip **7**, 1746–1751 (2007).
[15] T. Franke, L. Schmid, D. A. Weitz, and A. Wixforth, "Magneto-mechanical mixing and manipulation of picoliter volumes in vesicles," Lab Chip **9**, 2831–2835 (2009).
[16] Y. Gao, M. Hulsen, T. Kang, and J. den Toonder, "Numerical and experimental study of a rotating magnetic particle chain in a viscous fluid," Phys. Rev. E **86**, 041503 (2012).
[17] A. Vázquez-Quesada and M. Ellero, "Rheology and microstructure of non-colloidal suspensions under shear studied with smoothed particle hydrodynamics," J. Non-Newtonian Fluid Mech. **233**, 37–47 (2016).
[18] C. E. Sing, L. Schmid, M. F. Schneider, T. Franke, and A. Alexander-Katz, "Controlled surface-induced flows from the motion of self-assembled colloidal walkers," Proc. Natl. Acad. Sci. U. S. A. **107**, 535–540 (2010).
[19] M. Doi and S. F. Edwards, *The Theory of Polymer Dynamics* (Oxford University Press, 1988), Vol. 73.
[20] C. Wilhelm, J. Browaeys, A. Ponton, and J.-C. Bacri, "Rotational magnetic particles microrheology: The Maxwellian case," Phys. Rev. E **67**, 011504 (2003).
[21] S. Kim and S. J. Karrila, *Microhydrodynamics: Principles and Selected Applications* (Dover Publications Inc., 2005).
[22] X. Hu and N. Adams, "Angular-momentum conservative smoothed particle dynamics for incompressible viscous flows," Phys. Fluids **18**, 101702 (2006).
[23] P. Español and M. Revenga, "Smoothed dissipative particle dynamics," Phys. Rev. E **67**, 026705 (2003).
[24] J. P. Morris, P. J. Fox, and Y. Zhu, "Modeling low Reynolds number incompressible flows using SPH," J. Comput. Phys. **136**, 214–226 (1997).
[25] M. Ellero and N. A. Adams, "SPH simulations of flow around a periodic array of cylinders confined in a channel," Int. J. Numer. Methods Eng. **86**, 1027–1040 (2011).
[26] J. J. Monaghan, "Simulating free surface flows with SPH," J. Comput. Phys. **110**, 399–406 (1994).
[27] X. Bian, S. Litvinov, R. Qian, M. Ellero, and N. A. Adams, "Multiscale modeling of particle in suspension with smoothed dissipative particle dynamics," Phys. Fluids **24**, 012002 (2012).
[28] A. Vázquez-Quesada, X. Bian, and M. Ellero, "Three-dimensional simulations of dilute and concentrated suspensions using smoothed particle hydrodynamics," Comput. Part. Mech. **3**, 167–178 (2016).
[29] X. Bian and M. Ellero, "A splitting integration scheme for the SPH simulation of concentrated particle suspensions," Comput. Phys. Commun. **185**, 53–62 (2014).
[30] S. Litvinov, M. Ellero, X. Hu, and N. Adams, "A splitting scheme for highly dissipative smoothed particle dynamics," J. Comput. Phys. **229**, 5457–5464 (2010).
[31] D. Dratler and W. Schowalter, "Dynamic simulation of suspensions of non-brownian hard spheres," J. Fluid Mech. **325**, 53–77 (1996).
[32] J. F. Brady and J. F. Morris, "Microstructure of strongly sheared suspensions and its impact on rheology and diffusion," J. Fluid Mech. **348**, 103–139 (1997).
[33] S. Litvinov, M. Ellero, X. Hu, and N. Adams, "Self-diffusion coefficient in smoothed dissipative particle dynamics," J. Chem. Phys. **130**, 021101–021104 (2009).